SolarPACES 2022, 28th International Conference on Concentrating Solar Power and Chemical Energy Systems
Receivers and Heat Transfer Media and Transport: Point Focus Systems
https://doi.org/10.52825/solarpaces.v1i.714

Published: 19 Mar. 2024

Influence of Temperature on Properties and Dynamics of Gas-Solid Flow in Fluidized-Particle Tubular Solar Receiver

Ronny Gueguen[1][https://orcid.org/0000-0002-5236-8638], Guillaume Sahuquet[1][https://orcid.org/0000-0003-0275-2890], Jean-Louis Sans[1], Samuel Mer[1][https://orcid.org/0000-0001-7915-3146], Adrien Toutant[1][https://orcid.org/0000-0002-7156-1732], Françoise Bataille[1][https://orcid.org/0000-0003-4470-8636], and Gilles Flamant[1][https://orcid.org/0000-0003-4562-8515]

[1] Processes, Materials and Solar Energy laboratory (PROMES) – CNRS, France

Abstract. A fluidized particle single-tube solar receiver has been tested for investigating the gas-particle characteristics that enable the best operating conditions in a commercial-scale plant. The principle of the solar receiver is to fluidize the particles in a vessel – the dispenser – in which the receiver tube is plunged. The particles are flowing upward in the tube, irradiated over 1-meter height, by applying an overpressure in the dispenser. Experiments with a concentrated solar flux varying between 188 and 358 kW/m² are carried out, and the particle mass flux varied from 0 to 72 kg/(m²s). The mean particles and external tube wall temperatures in the irradiated zone are heated from the ambient to respectively 700°C and 940°C. It is shown that the temperature rise leads to a decrease of the particle volume fraction. Furthermore, a self-regulation of the system is evidenced with a short transient regime. This characteristic is essential from the operational viewpoint. The thermal efficiency of the receiver increases with the particle flow rate, reaching between 60 and 75% above 30 kg/(m²s). Several fluidization regimes are identified thanks to pressure signal analyses, like slugging, turbulent and fast fluidization, showing that regimes transitions are strongly affected by the temperature.

Keywords: Concentrated Solar Power, Particles Solar Receiver, Fluidized Particles.

Introduction

Concentrated solar power (CSP) plants convert solar radiation into electricity. A key component of the plant is the solar receiver, in which the heat transfer fluid (HTF) absorbs the solar radiation and transfers thermal power to the heat conversion units. The most commonly used HTF in commercial solar towers is molten salt. It has a maximum operating temperature limited to around 560°C, which constrains the receiver outlet temperature and thus the heat-to-power cycle efficiency. To overcome this issue, several solar receiver technologies using particles are developed worldwide. Particularly, the centrifugal receiver (DLR, Germany) [1], the falling particles receiver (Sandia, USA) [2], and the fluidized particle-in-tube receiver (CNRS, France) [3] are developed at pilot scale. For the latter, outlet particle temperature up to 750°C was demonstrated, that enables implementing high efficiency heat-to-electricity thermodynamic conversion cycles [4]. One of the main characteristics of this technology is the occurrence of several fluidization regimes depending on the operating conditions with various particle volume fractions and particle mixing that directly governs the heat transfer in such a solar receiver. However, the fluidization regimes have not been explored during the previous on-sun experimental campaigns [5] and the influence of temperature on these regimes is poorly detailed in the literature. Bubbling, slugging, turbulent fluidization and fast fluidization regimes have been

identified in the receiver at ambient temperature [6,7]. The turbulent fluidization regime being associated to high wall-to-fluidized particle heat transfer coefficient [8], it should be favored to improve the solar receiver performances. Experiments are conducted with a single-tube receiver at the CNRS 1 MW solar furnace (France) with various solar flux densities to quantify the influence of the temperature on the gas-particle suspension behavior.

Experimental Set-Up

The solar receiver is composed of a single Inconel tube, of 3 m height and 48 mm internal diameter. A schematic representation of the tube and its instrumentation is given in Figure 1a. The tube is immersed in a vessel (called “dispenser”) in which olivine particles of 61 µm mean diameter, belonging to the group A of the Geldart classification [9], are fluidized. The particles rise in the tube by applying both an overpressure in the dispenser and injecting a secondary air flow – called “aeration” – at 0.5 m height above the tube bottom tip. The aeration flow rate varies from 0.08 to 1.65 sm^3/h (standard cubic meters per hour). A weighing device is implemented at the outlet of the receiver tube to measure the particle mass flow rate, varying from 0 to 475 kg/h (i.e. 72 kg/(m^2s)). The receiver tube is irradiated over an one-meter interval, from 0.6 m to 1.6 m above the aeration injector (yellow zone in Figure 1a), with concentrated solar flux densities varying in the range 188 – 358 kW/m^2 depending on the aiming strategy of the heliostats. The irradiated part of the tube is surrounded by a refractory cavity (white part in Figure 1b). K-type thermocouples and pressure probes are implemented to determine fluidization characteristics such as the particle volume fraction (α) and to identify the fluidization regimes thanks to pressure signal processing methods [7]. In particular, three well-instrumented sections in terms of internal and external (i.e. welded) thermocouples delimitate the irradiated part (in green in Figure 1a). Details about the used pressure sensors and flowmeters are given in [7]. 187 experiments have been performed, and the associated results are presented in the following section.

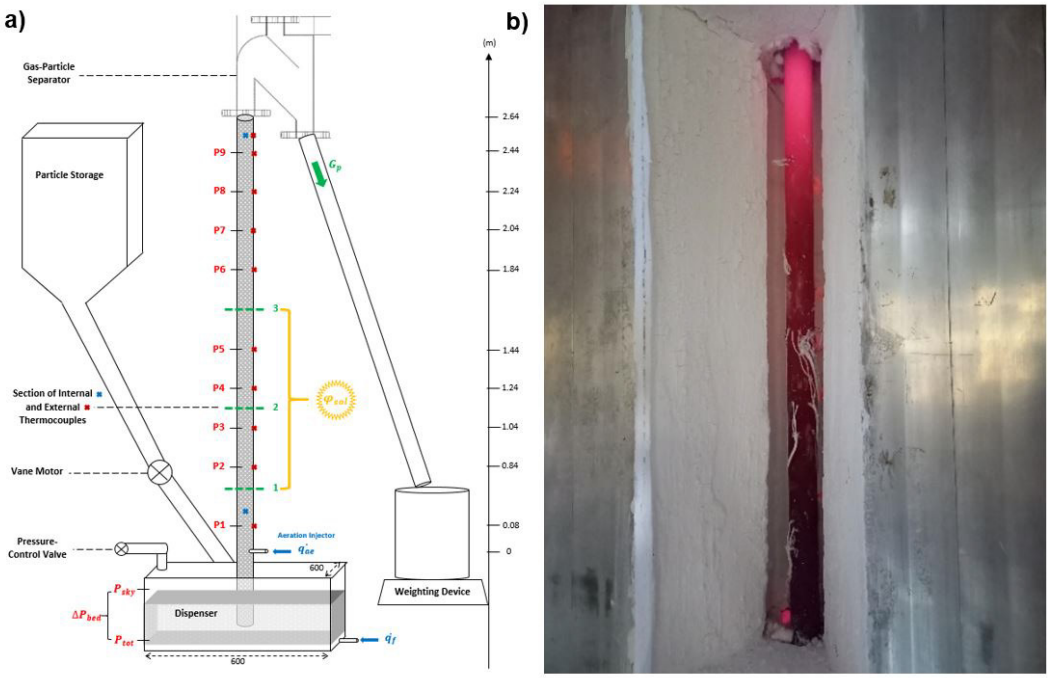

Figure 1. a) Schematic representation of the solar receiver and its instrumentation, with the irradiated zone delimited in yellow, and b) Picture of the irradiated part of the receiver tube – still hot – after an experiment.

Results and Discussion

Particle Volume Fraction

The particle volume fraction in the receiver tube, α, is calculated based on the measurement of the pressure drop between two pressure probes (ΔP) with Equation 1, neglecting pressure drops due to particle acceleration and friction [6]. In Eq. 1, Δh is the distance between the probes, and ρ indicates the densities of the olivine particles (3300 kg/m^3) and of air. α_{av} is calculated as an average of the local volume fractions measured at various heights, averaged over the acquisition time. Figure 2 presents the evolution of α_{av} as a function of the superficial aeration velocity U_{ae} – i.e. the aeration flow rate divided by the internal tube cross-sectional area (S_t), taking temperature and pressure into account – for two particle mass fluxes G_p (the particle mass flow rate normalized by S_t). The various markers and colors represent the mean particle temperature measured in the irradiated zone.

$$\alpha = \Delta P / \left(\left(\rho_{part} - \rho_{air} \right) g \Delta h \right) \quad (1)$$

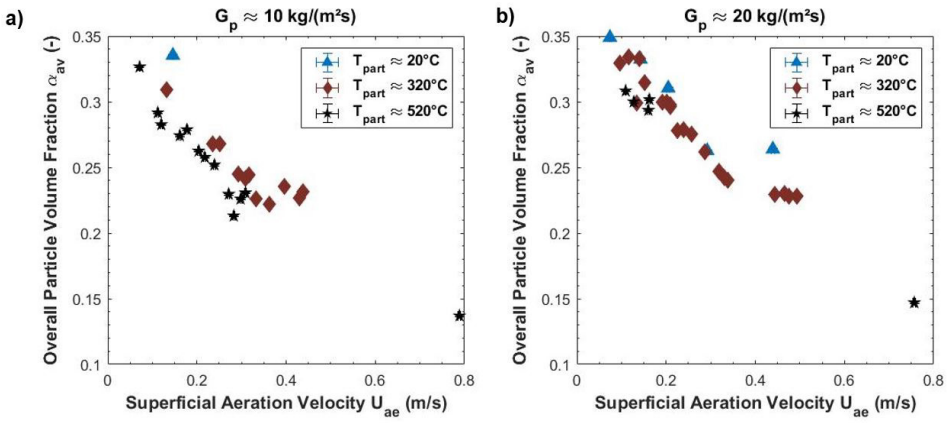

Figure 2. Overall particle volume fraction as a function of aeration velocity with the mean particle temperature as parameter, with a particle mass flux of approximately a) 10 and b) 20 kg/(m²s).

Increasing the air velocity – i.e. the aeration flow rate – results in a decrease of the particle volume fraction, while an increase of the particle mass flux leads to an increase of α_{av} due to supplementary pressure drops, as previously observed in [7]. Furthermore, increasing the temperature leads to a decrease of the particle volume fraction, for a given aeration flow rate. This behavior is likely due to the decrease of the air density with temperature (from approximately 1 kg/m^3 at 25°C at the altitude of the experiments to approximately 0,38 kg/m^3 at 520°C), leading in conjunction to an increase of the air velocity. Taking this influence into account enables better gathering the experimental points but not enough to have a single trend, meaning that the temperature effect on the particle volume fraction is not only due to the air velocity. Experiments with higher particle mass fluxes and solar fluxes are in progress to improve the understanding of this temperature effect.

Transient behavior of the system, autoregulation capacity of the fluidized particle-in-tube receiver

The variations of the particle volume fraction induced by variations of the aeration velocity enable precisely controlling the particle mass flux during operation, as illustrated in Figure 3. The overpressure in the dispenser, named "P_{tot}" (in black), was fixed during the experiment at approximately 305 mbar, and the concentrated solar flux density (in yellow) was constant at 230 kW/m² along the tube (1 m). The aeration flow rate – represented in blue in term of the

aeration velocity U_{ae} calculated with the mean particle temperature – was progressively increased, from 0.16 to 0.55 sm^3/h. Consequently, the particle mass flux (G_p) increased, as shown by the slope changes of the temporal evolution of the particle mass flowing out the tube measured with the weighing device (in green). The particle mass flux and temperature (in red) variations and successive steady states are represented in Figure 3 with green dashed lines.

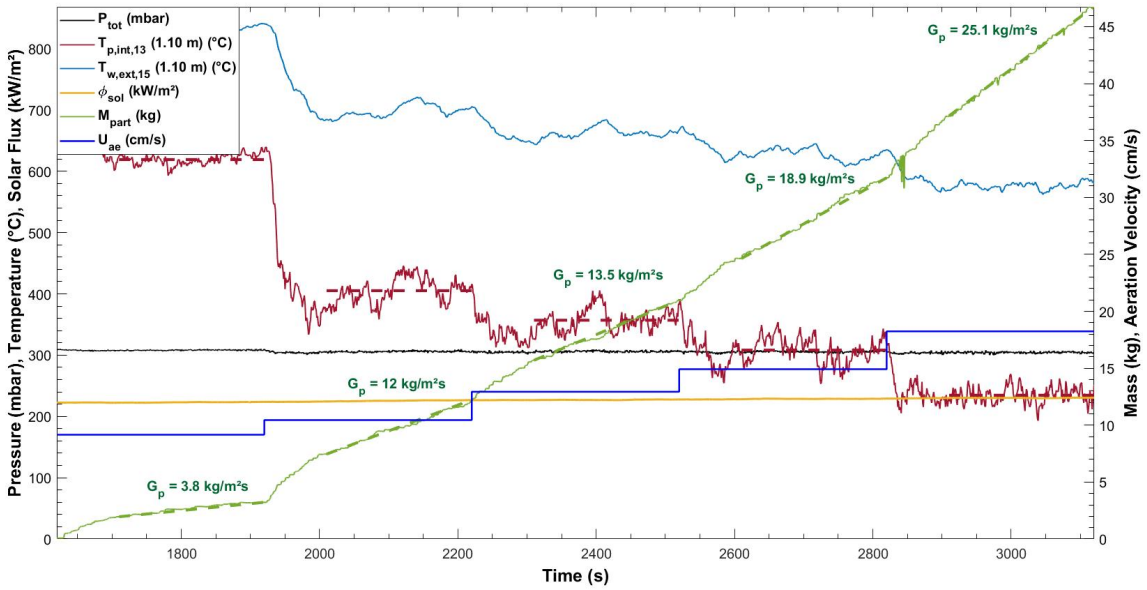

Figure 3. Temporal evolutions of the particle temperature and mass flux, due to variations of the aeration flow rate. P_{tot} (black) is the overpressure in the dispenser, $T_{p,int,13}$ (red) and $T_{w,ext,15}$ (blue) are respectively the particle and wall temperatures at the middle of the irradiated zone, Φ_{sol} (yellow) is the incident concentrated solar flux, M_{part} (green) is the particle mass in the weighing device, and U_{ae} (blue) is the superficial aeration velocity calculated with the mean particle temperature.

Accounting for the data in Figure 2, for a given pressure imposed in the dispenser and a constant solar flux density on the receiver tube, the transient sequence can be summarized as follows.

Aeration flow rate increase ⇒ particle volume fraction decrease ⇒ particle mass flux increase (α in the tube is proportional to P_{tot} in first approximation, then a decrease of α results in an increase of G_p at constant pressure) ⇒ particle temperature decrease (an increase of G_p at constant Φ_{sol} leads to an increase of the extracted thermal power, then a decrease of T_p) ⇒ particle volume fraction increase (cf. Figure 2) ⇒ new steady state (G_p and T_p) corresponding to the equilibrium value of the mean particle volume fraction $\alpha(T_p)$.

The sequence last approximately 90 seconds. The opposite variations of α due to the experimental parameters highlight a self-regulation of the system.

During operation, an increase of the DNI increases the particle temperature. The new steady state corresponds to a higher particle mass flow rate due to the increase of the air velocity. Now, let us imagine a decrease of the DNI, because of clouds for example. It will lead to a decrease of the air velocity. This phenomenon has been simulated by decreasing the aeration flow rate, as represented in Figure 4. The initial steady state is the following. A pressure in the dispenser and a concentrated solar flux density of respectively 230 mbar and 200 kW/m², and an aeration flow rate of 0.99 sm^3/h. As a consequence, particles are flowing in the receiver with a mass flux of 14.1 kg/(m²s) and a mean temperature of 305°C. At a time of 1680 seconds, the aeration flow rate is decreased to 0.66 sm^3/h, inducing a stop of the particle flow,

hence an increase of the particle temperature. Then, the autoregulation sequence led to a decrease of α and progressively a restart of the particle flow, avoiding overheating of the absorber wall. Here the autoregulation sequence last 440 seconds (~ 7 minutes).

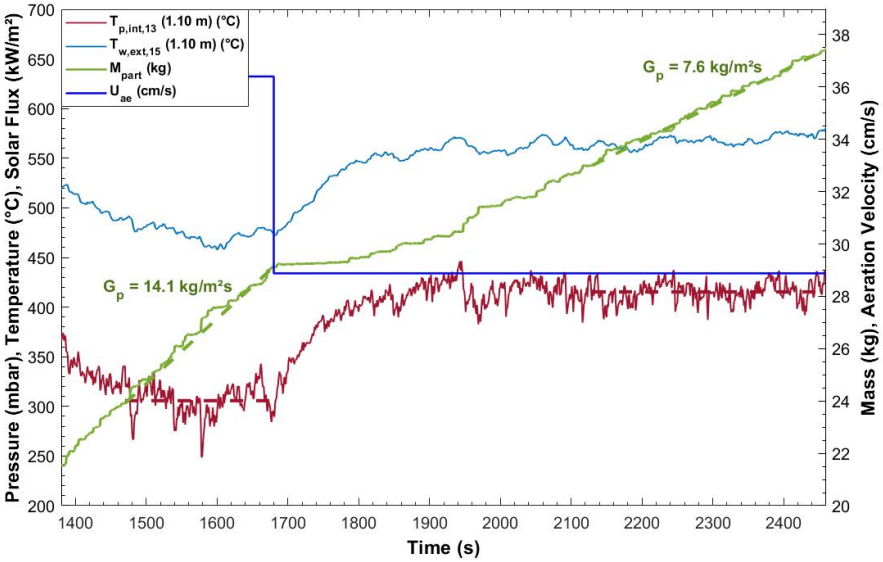

Figure 4. Temporal evolutions of the particle temperature and mass flux, due to variations of the aeration flow rate at 1680 seconds. Experimental parameters are represented in the same way as in Figure 3.

Receiver efficiency

Equation 2 calculates the extracted power by the particles, Φ_{part}. In the equation, $\dot{m_{part}}$ is the particle mass flow rate, in kg/s, and Cp_{part} is the heat capacity of the olivine, of approximately 1 kJ/(kg.K) in the measured temperature range. It is precisely calculated according to [5] with the mean particle temperature in the irradiated zone of the receiver as the reference. Finally, $T_{part,out}$ and $T_{part,in}$ are the particle temperatures measured respectively at the outlet of the irradiated zone – at the tube center – and in the dispenser. The thermal efficiency of the system, η, is the ratio of the extracted power to the incident solar power (Φ_{sol}) as shown in Equation 3. Figure 5 presents the variation of the receiver efficiency with the particle mass flux for four incident solar flux densities on the tube. The error bars are calculated as the classical error propagation from Eqs. 2 and 3, due to the measurement error on the temperatures, particle mass flow rate and incident solar power.

$$\Phi_{part} = \dot{m_{part}} Cp_{part} \left(T_{part,out} - T_{part,in}\right) \quad (2)$$

$$\eta = \Phi_{part} / \Phi_{sol} \quad (3)$$

The thermal efficiency of the receiver increases with the particle mass flux and reaches a plateau, for a given solar flux density. Above 30 kg/(m^{2}s), it ranges between 60 and 75 %. The low values of η at low particle mass fluxes are due to the high temperatures of the particles and the tubes that lead to high radiative losses [10]. Simultaneously, the particle temperature decreases with G_p, and reaches between 100 and 350 °C above 30 kg/(m²s) depending on the incident solar flux. More generally, the heat losses are due to thermal radiation emission, convection around the tube and to fluidization gas. Fluidization gas loss accounts only for 2-3 %.

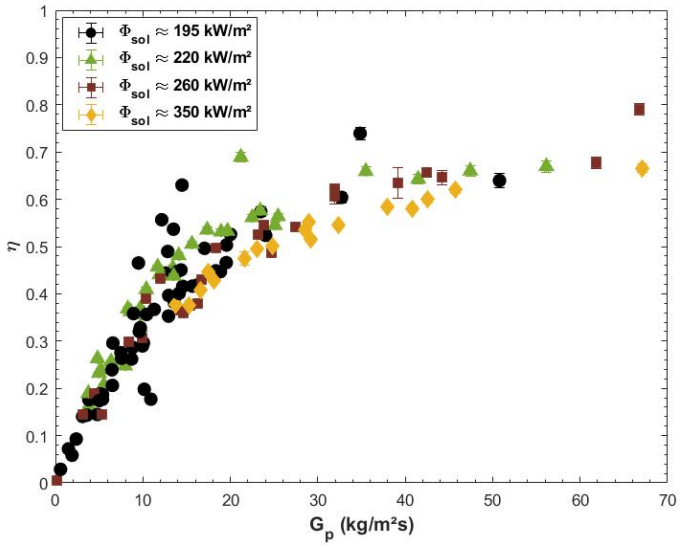

Figure 5. Evolution of the thermal efficiency of the system as a function of the particle mass flux and the incident solar flux density.

Fluidization regimes

The fluidization regimes in the receiver tube are identified with temporal pressure signals processing methods [7]. One of the main methods is the coherence analysis, described in [11], that consists of applying a Fast Fourier Transform on a temporal pressure signal to compute a power spectrum. The frequencies distribution, and both the frequency and the magnitude of the dominant frequency are good indicators of the fluidization regimes [7]. Figure 6 illustrates an example of two temporal pressure signals, measured in similar conditions at a height of 1.44 m above the aeration injector (i.e. in the middle of the irradiated zone): an aeration velocity of 0.15 m/s, and a particle mass flux of respectively 13 and 14 kg/(m²s).

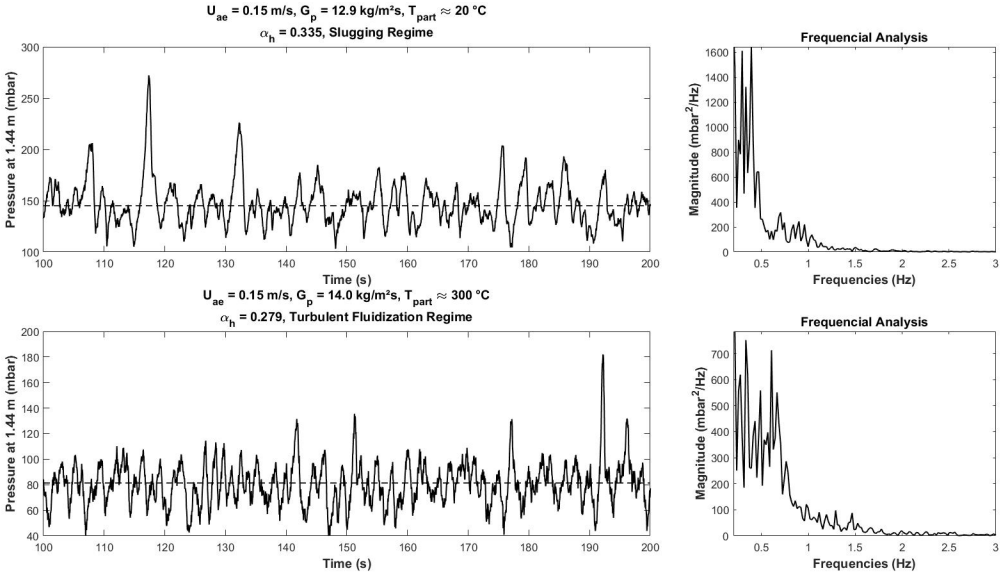

Figure 6. Examples of two temporal pressure signals and the corresponding frequency analyses measured for similar experimental parameters (aeration velocity of 0.15 m/s and particle mass fluxes of 12.9 and 14 kg/(m²s)). The particle temperatures are respectively 20 and 300°C.

The main difference between these two examples is the particle temperature. The first one (first line in Figure 6) has been realized at ambient temperature, without concentrated solar

flux. At ambient temperature, the overall particle volume fraction is 0.335, and the coherence analysis enables obtaining the power spectrum presented at the right top of Figure 6, corresponding to the slugging regime. The second spectrum (second line in Figure 6) has been obtained with a concentrated solar flux density of 190 kW/m², leading to a particle temperature of approximately 300°C. Consequently, the overall particle volume fraction decreased to ~0.28, Furthermore, the corresponding spectrum obtained is characteristic of the turbulent fluidization regime induced by the air velocity increase due to the fluidized bed temperature increase. It means that the transition air velocities between the fluidization regimes are affected by temperature. This finding was expected because previous studies showed that the velocity triggering the turbulent fluidization regime in a classical fluidization column decreases with temperature [12]. Supplementary experiments are in progress with higher solar flux densities in order to determine precisely this effect, accounting for all the fluidization regimes observed.

Conclusion

Experiments were performed with the fluidized particle-in-tube solar receiver at the 1-MW solar furnace of CNRS, Odeillo (France) using large ranges of the experimental parameters. The aeration flow rate varies from 0.08 to 1.65 sm^3/h, corresponding to superficial air velocity in the tube from 0.02 to 0.77 m/s by taking into account the particle temperature. The concentrated solar flux ranges between 188 and 358 kW/m². Consequently, the particles are heated up to approximately 700°C, and the particle mass flux ranges between 0 and 72 kg/(m²s), corresponding to a mass flow rate of 475 kg/h. The main conclusions are the following.

The increase of the temperature leads to a decrease of the particle volume fraction, for given aeration and particle flow rates. The influence of the temperature results in a self-regulation of the system. A variation of one of the operating parameters leads to instantaneous response of the particle volume fraction, mass flux and temperature, until a new steady state is reached. The thermal efficiency of the receiver increases with the particle mass flux, reaching between 60 and 75% above 30 kg/(m²s) in the tested operation parameters range. Finally, several fluidization regimes triggered by the fluidized bed temperature have been observed, from the slugging to the turbulent fluidization.

In operating conditions of a solar plant, the experimental results indicate that, first, the aeration flow rate enables a fine control of the system control in terms of particle mass flow rate, temperature and fluidization regimes; and second, the self-regulation properties of the system avoid overheating of the absorber wall. Supplementary experiments are in progress with higher particle flow rates and concentrated solar fluxes to study more precisely the influence of particle temperature on the gas-particle suspension behavior and to measure the heat transfer coefficients associated with the various fluidization regimes.

Data availability statement

The data supporting the results can be accessed asking the authors.

Author contributions

Conceptualization, Supervision, Resources and Funding acquisition: G.F. Methodology, Software, Investigation and Writing – original draft: R.G. Validation, Formal Analysis and Writing – review and editing: S.M., A.T., F.B. and G.F. Data curation: G.S, J.L.S and R.G.

Competing interests

The authors declare no competing interests.

Funding

This work was funded by the French “Investments for the future” (“*Investissements d’Avenir*” program managed by the National Agency for Research (ANR) under contract ANR-10-LABX-22-01 (labex SOLSTICE) and the U.S. Department of Energy, Solar Energy Technologies Office under Award Number 34211.

Acknowledgement

The authors want to thank Michael Tessoneaud for all the help managed with the experiments, and Roger Garcia for the conception of the mock-up.

References

1. W. Wu, L. Ambseck, R. Buck, R. Uhlig, R. Ritz-Paal, “Proof of concept test of a centrifugal particle receiver” Energy Procedia, 49, pp. 560–568, 2014, doi: 10.1016/j.egypro.2014.03.060.
2. C. K. Ho, J. Christian, J. Yellowhair, S. Jeter, M. Golob, C. Nguyen, K. Repole, S. Abdel-Khalik, N. Siegel, H. Al-Ansary, A. El-Leathy, B. Gobereit, “Highlights of the high-temperature falling particle receiver project: 2012-2016”, AIP Conference Proceeding, 1850, 030027, 2017, doi: 10.1063/1.4984370.
3. G. Flamant, D. Gauthier, H. Benoit, J. L. Sans, R. Garcia, B. Boissière, R. Ansart, M. Hemati, “Dense suspension of solid particles as a new heat transfer fluid for concentrated solar thermal plants: On-sun proof of concept”, Chemical Engineering Science, 102, pp. 567–576, 2013, doi: 10.1016/j.ces.2013.08.051.
4. M. T. Dunham, B. D. Iverson, “High-efficiency thermodynamic power cycles for concentrated power systems”, Renewable and Sustainble Energy Reviews, 30, pp. 758–770, 2014, doi: 10.1016/j.rser.2013.11.010.
5. A. Le Gal, B. Grange, M. Tessonneaud, A. Perez, C. Escape, J. L. Sans, G. Flamant, “Thermal analysis of fluidized particle flows in a finned tube solar receiver”, Solar Energy, 191, pp. 19–33, 2019, doi: 10.1016/j.solener.2019.08.062.
6. R. Gueguen, G. Sahuquet, S. Mer, A. Toutant, F. Bataille, G. Flamant, “Fluidization Regimes of Dense Suspensions of Geldart Group A Fluidized Particles in a High Aspect Ratio Column”, Chemical Engineering Science, 118360, 2022, doi: 10.1016/j.ces.2022.118360.
7. R. Gueguen, G. Sahuquet, S. Mer, A. Toutant, F. Bataille, G. Flamant, “Gas-Solid Flow in a Fluidized-Particle Tubular Solar Receiver: Off-Sun Experimental Flow Regimes Characterization”, Energies, 14, 7392, 2021, doi: 10.3390/en14217392.
8. S. Y. Wu, J. Baeyens, “Effect of operating temperature on minimum fluidization velocity”, Powder Technology, 67, pp. 217–220, 1991, doi: 10.1016/0032-5910(91)80158-F.
9. D. Geldart, “Types of Gas Fluidization”, Powder Technology, 7, pp. 285–292, 1973, doi: 10.1016/0032-5910(73)80037-3.
10. R. Gueguen, B. Grange, F. Bataille, S. Mer, G. Flamant, “Shaping High Efficiency, High Temperature Cavity Tubular Solar Central Receivers”, Energies, 13, 4803, 2020, doi: 10.3390/en13184803.
11. J. Van der Schaaf, J. C. Schouten, F. Johnsson, “Non-intrusive determination of bubble and slug length scales in fluidized beds by decomposition of the power spectral density of pressure time series”, International Journal of Multiphase Flow, 28, pp. 865–880, 2002, doi: 10.1016/S0301-9322(01)00090-8.
12. H. T. Bi, N. Ellis, I. A. Abba, J. R. Grace, “A state-of-the-art review of gas-solid turbulent fluidization”, Chemical Engineering Science, 55, pp. 4789–4825, 2000, doi: 10.1016/S0009-2509(00)00107-X.